Faculty and Researchers | Faculty and Researchers' Publications

2017

On the structure and dynamics of stratified wakes generated by submerged propagating objects

Moody, Zachary E.; Merriam, Christopher J.; Radko, Timour; Joseph, John

Taylor & Francis

Taylor & Francis
Taylor & Francis Group

Check for updates

On the structure and dynamics of stratified wakes generated by submerged propagating objects

Zachary E. Moody, Christopher J. Merriam, Timour Radko 🅭 and John Joseph 🅭

Oceanography Department, Naval Postgraduate School, Monterey, CA, USA

ABSTRACT

The structure and intensity of the intermediate wake generated by a submerged propagating body in a stratified fluid was studied using a combination of (i) numerical simulations, (ii) field measurements, and (iii) laboratory experiments. The numerical component offered guidance for the field work performed in Monterey Bay (CA, USA) in the summer of 2015. The field work focused on subsurface thermal signatures of a submerged propagating object. Vertical temperature profiles suggested that long-term changes in thermal stratification can occur after the passage of a towed body. Horizontal temperature variability, measured by an autonomous underwater vehicle facilitated the identification of the wake using perturbation temperature variance as the key diagnostic variable. Analogous thermal signatures of stratified wakes were found in ocean observations and in modelling results. The influence of the tow ship on the wake was shown to be minimal. Laboratory experiments focused on the surface expression of stratified wakes were used to complement numerical simulations and field measurements. All three components of this project indicate that detection of the wake of a submerged object based on its thermal signatures is a viable and effective approach.

1. Introduction

As an object is moving through a stratified water column, it inevitably generates a wake due to the transfer of momentum. Several critical features of the wake result from the interaction between inertial and buoyancy forces. These dynamics are controlled by the Froude number (Fr)

$$Fr = \frac{U}{ND}, \qquad (1)$$

where U is the velocity, $N = \sqrt{-(g/\rho)(\partial\sigma/\partial z)}$ is the Brunt–Väisälä frequency (g, ρ, and σ are the gravity, reference and potential densities respectively) and D is diameter of the submerged object. When the Froude number is small, the laminar flow pattern can be described by standard techniques of linear perturbation theory (e.g. Radko 2001). In this limit, the wake is confined to a persistent angle of 19°28′ and the magnitude of perturbation depends sensitively on the stratification pattern. When the Froude number exceeds unity, the wake tends to be more disorganised and turbulent. If the fluid were homogenous, the signature would be limited to velocity perturbations and would diffuse more rapidly (Schooley & Stewart 1963).

The non-dimensional parameter measuring the significance of effective viscosity on the wake dynamics is the Reynolds number

$$Re = \frac{UD}{\nu}, \qquad (2)$$

where ν is the molecular viscosity of seawater. In the context of direct numerical simulations (DNS) (Section 2), ν in Equation (2) is replaced by the effective viscosity (A_H) used by the numerical model. The elevated viscosity is commonly used in models to control numerical instability and to resolve the dissipation scale of turbulence.

Another important non-dimensional parameter, which measures the influence of the sea-surface on the wake pattern, is the depth ratio (d_r)

$$d_r = \frac{H}{D}, \qquad (3)$$

where H is the submerged body (SB) depth, defined in this study as the distance from the axis of SB to the sea-surface, and D is the SB's diameter. The depth ratio also plays a major role in evaluating the potential for wake detection based on its thermal surface signatures. The summary of relevant parameters is given in Table 1.

Table 1. Typical scales of key variables realised in the field and laboratory experiments, and in operational scenarios.

	Monterey Bay experiment	Laboratory experiment	Typical operational conditions
U_0	3 m/s	0.5 m/s	10 m/s
N	$6 \cdot 10^{-3} \, \text{s}^{-1}$	$6.5 \cdot 10^{-2} \, \text{s}^{-1}$	$3 \cdot 10^{-3} \, \text{s}^{-1}$
D	1 m	4.25 cm	10 m
Fr	500	180	300
Re	$3 \cdot 10^6$	$2 \cdot 10^4$	$1 \cdot 10^8$
H	15 m	12 cm	50–300 m
d_r	15	2.82	5–30

Wake development is comprised of three phases. Relatively high velocities and turbulent mixing mark the first phase – the near wake. During the near wake phase, the largest vertical perturbations of mass and momentum force a turbulent wake signature to expand three-dimensionally until it is fully developed with the onset of the intermediate wake (Redford et al. 2015). With the onset of the intermediate (or non-equilibrium) phase, buoyancy forces exert control to reduce vertical motions while horizontal motions continue to expand, resulting in a vertically flattened and horizontally stretched wake signature. The final phase, the late wake, is characterised by dissipation of small-scale perturbations and formation of isolated coherent vortices (Meunier & Spedding 2004). The length of each phase is controlled by the buoyancy frequency N, but can be affected by other environmental conditions and towed SB characteristics. Research activities discussed in our present communication were focused on the intermediate wake phase and, more specifically, thermal signatures of the wake produced behind a SB.

A towed SB can generate wake patterns that are different from those of a self-propelled SB. The mean velocity and shear generated from momentum transfer of a towed body will persist longer than for the self-propelled case (de Stadler & Sarkar 2012). However, even with large self-propelled underwater objects, the potential exists to detect vortex patterns from the late wake for up to 12 days in the open ocean (Spedding et al. 1996). Voropayev et al. (2012) has shown that surface ship wakes can be sensed using an infrared (IR) camera to distinguish propeller upwelled water up to 1°C cooler than adjacent surface waters temperatures. Using laboratory experiments and theoretical arguments, Voropayev et al. (2007), Spedding et al. (1996), and Spedding (2014) have also shown that, under the right conditions, the momentum signature from a self-propelled SB can extend to the sea-surface with measurable magnitude. The in situ oceanographic measurements of wake properties are much more rare and precious. Of direct relevance to our study are the observations of Fiekas (1997), who measured the temperature distribution across the submarine wake using a towed array of sensors. Strong temperature anomalies

of ~0.5°C caused by the passage of a submarine were recorded after it moved the distance of 1.5 km from the observational site. Such findings motivate the development of new detection algorithms that are based on thermal signatures of stratified wakes.

The present study provides a comprehensive analysis of wake intensity and persistence using a combination of (i) numerical simulations, (ii) field observations conducted in Monterey Bay, and (iii) laboratory experiments. The numerical simulation represents a towed SB and the diagnostics suggest feasibility of detection by means of temperature perturbations. These findings are tested in the ocean using a SB towed by a vessel to produce a wake in a thermally stratified environment. Field work incorporated naturally occurring variability which is not seen in a laboratory setting or captured by numerical models. Another advantage of the in situ oceanographic observations relative to their numerical and laboratory counterparts is the closer proximity of governing non-dimensional parameters (Fr, Re) to their operational targets (Table 1). For instance, both simulations (e.g. de Stadler & Sarkar 2012; Redford et al. 2015) and lab experiments (e.g. Voropayev & Smirnov 2003; Voropayev et al. 2007) generally deal with relatively viscous systems, characterised by Reynolds numbers which do not exceed $5 \cdot 10^4$. Free from numerical and laboratory constraints, our field experiments make it possible to extend this range by approximately two orders of magnitude (Table 1). Those values are still less than could be realised at the operational level ($Re \sim 10^8$). However, the major increase in Reynolds numbers achieved in our field measurements instils some confidence that our results represent the effectively inviscid 'hard turbulence' limit. The analysis of our numerical simulations and their comparison with field measurements suggests that, for the particular purpose of estimating perturbation temperature variance in the intermediate wake, frictional effects play a secondary role as long as Re is large. This conclusion, however, should not be taken for granted and should not be applied indiscriminately to other aspects of wake dynamics (e.g. its dissipation characteristics and long-term evolution).

While the general concept of hydrodynamic detection is known to the undersea warfare community, the at-sea quantification of key wake signatures in this study offers valuable operational guidance for development of effective detection strategies. Currently, reliable prognostic models do not exist for this type of detection due to the limited knowledge of intermediate wake patterns in the realistic oceanic environment. However, in view of continuous advancements of our understanding of wake dynamics and signatures, both empirical and theoretical, we are certain that accurate predictive

algorithms of this nature can be developed and implemented on the operational level.

2. Numerical simulations

In order to develop effective diagnostic techniques for the analysis of field measurements (Section 3), we first present numerical simulations of a wake generated by a towed body. The key strength of simulations is the availability of all information about the evolution of governing variables, which greatly reduces the ambiguity in the interpretation of observations.

2.1. Model, configuration, and resources

The Massachusetts Institute of Technology General Circulation Model (MITgcm) is a non-hydrostatic model that is highly scalable for parallel processing (Marshall et al. 1997), enabling it to accurately simulate the ocean environment around a propagating SB. For this study, MITgcm was run on the University of Texas at Austin's Advanced Computing Center (TACC) using Stampede, a Dell Powered Edge Cluster with Intel Xeon Phi coprocessors. The governing Navier–Stokes equations were solved using the finite volume technique. The choices of the horizontal velocity of the propagating object (U), as well as background exponential temperature (T) and linear salinity (S) gradients were based on conductivity, temperature, and depth (CTD) casts collected in Monterey Bay on 28 August 2016 (Figure 1) as follows:

$$T = 11.09 + (18.20 - 11.09) \exp(-0.08849 \cdot z), \quad (4)$$

$$S = \frac{-z - 6640}{-200}. \quad (5)$$

The modelled temperature profile starts at 18.20°C at the surface and exponentially decreases to 11.09°C at a depth of 30 m. The modelled salinity profile starts at 33.20 psu at the surface and linearly increases to 33.35 psu at 30 m depth. Since our simulations are focused on the interior wake structure, no attempt was made to model the surface mixed layer present in observations.

The model was configured to optimise computational efficiency by employing an exponential grid in the x and y directions. To better resolve perturbations generated by flow around the SB, the highest resolution was $\Delta x_0 = \Delta y_0 = 0.15$ m in the vicinity of the SB and exponentially increased to $\Delta x_1 = \Delta y_1 = 1.5$ m at the edges of the computational domain. A uniform grid was applied in the z-direction with $\Delta z = 0.15$ m in order to ensure high resolution for vertical perturbations. The size of computational domain was 1800 m in x, 150 m in y

and a depth of 30 m, and it was resolved by $N_x = 4096$, $N_y = 256$, and $N_z = 200$ grid points in x, y, and z respectively. The model setup is illustrated in Figure 1(a). The SB was represented by a 0.9 m diameter × 1.2 m length cylinder at 15 m depth moving with a horizontal velocity of 3 m/s. The SB's shape and dimensions were chosen to mimic the towed body used in the field component of our study (Section 3). The SB considered clearly falls in the category of bluff-body models. It should be realised that the bluff-body wakes can be substantially different from those generated by slender objects, elongated in the direction of motion (Lin & Pao 1979; Spedding 2014). In particular, bluff bodies tend to produce comparatively wider, more energetic – and thus more detectable – wakes, which may be beneficial at the present explorative stage of our investigation.

The simulations were performed in the coordinate system associated with the moving body. The inflow condition of 3 m/s at the left (negative x) boundary was implemented to represent the propagation of the SB relative to the ambient fluid. The Orlanski (1976) open boundary condition was implemented at the right (positive x) boundary to allow outflow from the domain and to avoid reverberation within the wake signature (Han et al. 1983). Periodic boundary conditions were assumed in the cross-flow direction (y) for all field variables. The free-slip rigid boundary condition was assumed at the bottom of the computational domain ($w(-H) = 0$) and the free surface boundary condition was used at the top.

Diffusivities of temperature and salinity, as well as kinematic viscosity were assigned uniform values: $A_H = 10^{-4}$ m^2/s was used for the horizontal dissipation, which corresponds to the Reynolds number of $Re \sim 3 \cdot 10^4$, and the vertical dissipation coefficients were $A_V = 10^{-5}$ m^2/s. This selection assured the numerical stability of the model as well as the adequate resolution of the dissipation scales of kinetic energy and thermal/haline variances. Our simulations exhibited very limited sensitivity to the chosen dissipation coefficients. For instance, doubling the values of (A_H, A_V) resulted in only 4% reduction of thermal variance (our key diagnostic variable) in the intermediate wake region. The time step of $\Delta t = 0.01$ s was used based on model resolution and horizontal velocity.

2.2. Model runs and diagnostics: synthetic Remote Environmental Monitoring Unit System (REMUS) approach

All model runs were integrated for 48 real-time computational hours on 512 processors to provide 480 s of data for the simulation presented here. Model output was recorded every 10 model seconds during the simulations
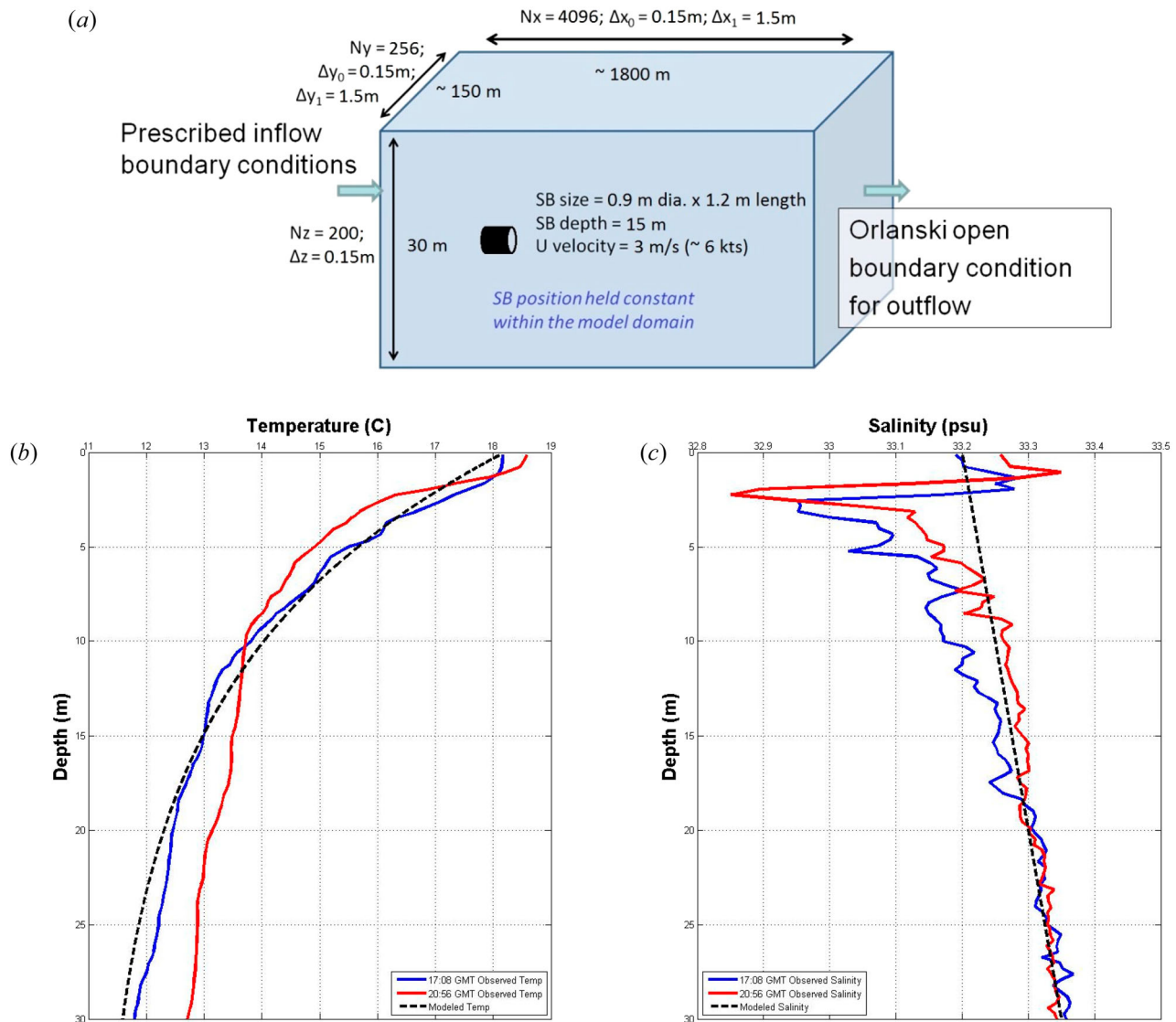
(a)

(b)

(c)

Figure 1. (a) Model configuration: grid-spacing, resolution, and boundary conditions. Temperature and salinity observations from CTD casts on 28 August 2016 in Monterey Bay, CA are plotted in (b) and (c) respectively, along with the corresponding background profiles used in simulations.

to produce the temperature fields used in this study. Vertical temperature perturbation is plotted in Figure 2(a) in order to determine the vertical extent of the SB wake. The horizontal temperature pattern at $H = 15$ m is plotted to reveal the extent of horizontal wake spreading (Figure 2(b)). Three-dimensional thermal perturbation in the range of 300–400 m behind SB passage is shown in Figure 3(a), revealing the highly turbulent nature of the flow in the wake.

In order to examine the wake signatures that are expected to be identified in the field experiment (Section 3) by the autonomous underwater vehicle (AUV), we have reconstructed the temperature time-series for a virtual sensor moving perpendicular to the wake at a uniform speed of 1.5 m/s. These time-series will be referred to as the synthetic REMUS data since they

represent a counterpart of the temperature signal sampled by the REMUS AUV used in the Monterey Bay experiment. For the fully developed wake at the model time of 480 s, the synthetic REMUS was launched with a depth of 15 m crossing at 450 m behind the SB at 75 m to the left of the wake. In 100 s, the synthetic REMUS crossed the turbulent wake, arriving at the point located at 75 m to the right of its axis.

The raw temperature data ($T(t)$) collected from this experiment (Figure 3(b)) were processed to quantify the levels of turbulence in the wake as follows. First, T was smoothed using a moving average filter over the time interval of 15 s. Next, the temperature perturbations (T') were calculated as the difference between the raw (T) and smooth data ($\bar{T}$). Finally, the perturbation temperature variance (T')^2 was also smoothed in time and

$\Delta T(x,z) = T - T_{bg}(z)$ at $y = 0$, $t = 480s$

(a)

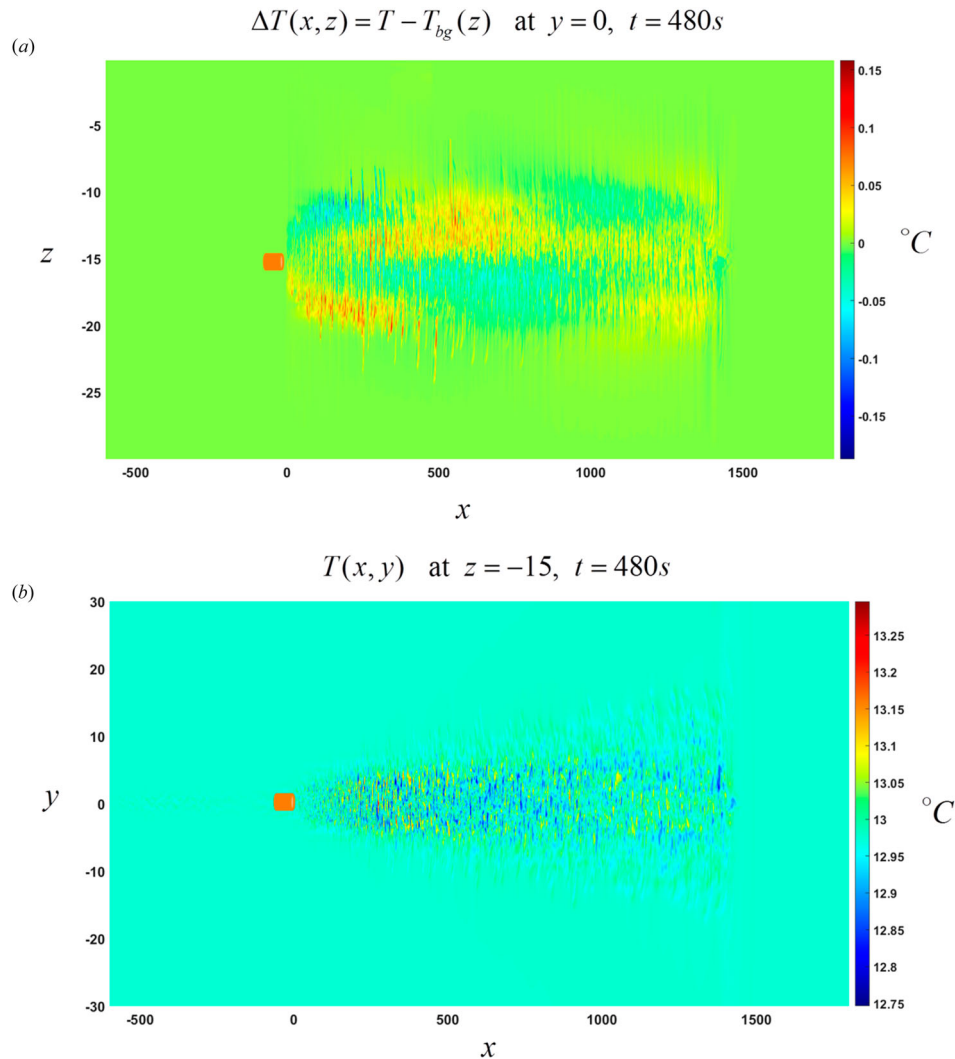$T(x,y)$ at $z = -15$, $t = 480s$

(b)

Figure 2. Vertical (a) and horizontal (b) sections of the temperature perturbation along the wake axes realised at $t = 480$ s of the numerical experiment.

converted to the root mean square temperature perturbation (Figure 3(c)):

$$T_{rms} = \sqrt{\overline{(T')^2}}. \tag{6}$$

All diagnostics are plotted in Figure 4(a). Synthetic REMUS time-series were reproduced for two additional wake crossings at distances of 600 and 750 m following the SB (Figure 4(b)). In all cases, we obtain a well-defined wake signature in terms of T_{rms} at easily detectable levels, providing essential guidance for the analysis of the following field experiments.

3. Field experiments

A field study was designed to examine the structure and detectability of a stratified wake generated by a tow body in Monterey Bay. The experiments were performed using research vessels moored at the Monterey Coast Guard

Pier (5 and 16 June) and at Moss Landing Harbor (28 August). The schedule was planned for summer days so that wind stress would be at a minimum, a shallower thermocline would be present, and overall weather conditions would be more suitable for boat operations. A towed body was built using a 121 litre trash can named 'Brute Grey' having a 0.67 m diameter. A second larger SB was constructed in a similar manner using a 435 litre capacity orange, jumbo waste container, appropriately named 'Agent Orange' and having a 0.89 m diameter (Figure 5). An RBR 100 m-rated pressure sensor and an Onset Hobo Pendant G tilt sensor were attached inside of each tow body.

3.1. Vertical temperature profiles

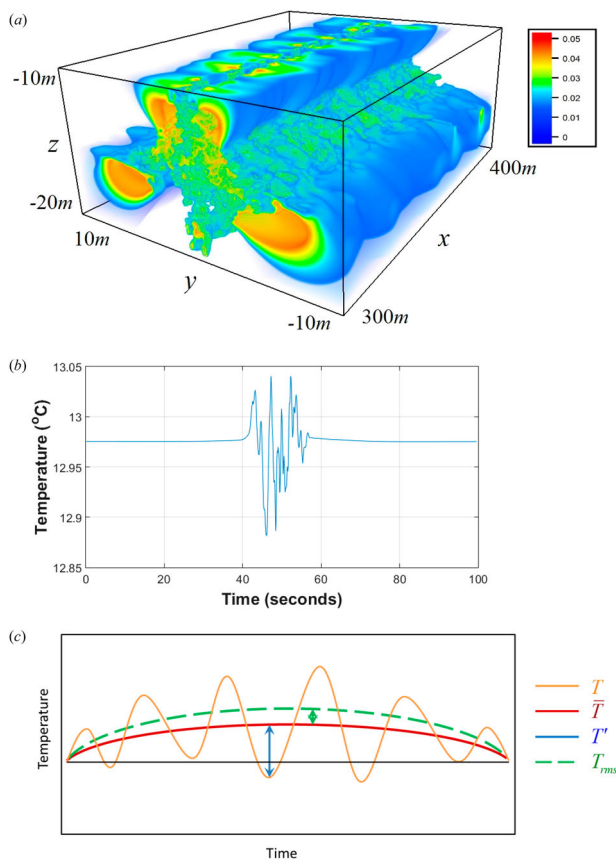On 5 June 2015, the first field experiment was conducted from the RV Fulmar for the purposes of testing the line

Figure 3. (a) The temperature perturbation generated by SB. (b) A typical example of temperature time-series obtained from the synthetic REMUS calculation. (c) Schematic of the diagnostic algorithm used to quantify the intensity of turbulence in the wake.

tension exerted by the tow body, collecting pressure and tilt sensor data, ensuring the integrity of the tow body, and collecting various Conductivity Temperature Depth (CTD) casts. Tilt data was examined to verify a level tow and pressure data was evaluated for the development of tow-depth/speed/tow-length characteristic curves. On the second day of field work, 16 June 2015, the experiment was conducted from the *RV Fulmar* as well, for the purposes of verifying and extending Brute Grey's tow characteristics curves up to speeds of 6 kt, testing line tension in a similar manner for Agent Orange prior to A-frame use, collecting pressure and tilt sensor data for both tow bodies, and conducting various CTDs.

A SonTek CastAway®-CTD was used to collect temperature vs. depth at various locations and times (Figure 5 (e)). This instrument is accurate to 100 m water depth using a rapid response thermistor to attain a measurement resolution of 0.01°C. It has a built-in GPS which references each cast with time and location. The instrument was attached to a line reel and allowed to free-fall at approximately 1 m/s to collect vertical temperature profiles. CTDs were conducted both inside and outside

of the vessel wake regions for comparison. Also, CTDs were cast in the vicinity of the tow tracks prior to and after the tows were completed to determine temporal changes in stratification.

On the first day of experimentation (5 June 2015), casts were taken inside of the wake region at 17:32 Greenwich Mean Time (GMT) and outside of it at 17:40 GMT following a tow run with Brute Grey at 43 m cable extension at a speed of 5 kt. CTD casts inside and outside of wake regions were also performed during the second field day (16 June 2015) with Agent Orange towed at 6 kt. Casts inside the wake region were repeated following an approximate 10 min wait in order to characterise wake residence time. During the final field day (28 August 2015), two CTD casts were performed in order to describe the environment prior to and following tow trials with REMUS experimentation. Interestingly for all three field days, CTDs from inside the wake showed a ∼0.5°C temperature increase at and above the target tow depth of 15 m. CTD casts from 5 June 2015 are displayed in Figure 6(a) with an undisturbed water column and following a 6 kt SB tow at 15.5 m depth.

The provisional explanation of the systematic increase in temperature at depth of SB after its passage is illustrated in Figure 6(b). Typical thermal stratification in Monterey Bay is represented by convex, non-uniformly increasing temperature profile with decreasing depth. As an SB passes through, it causes turbulence that mixes the seawater properties vertically. Over time, mixing causes the temperature profile to become more linear. While the net amount of heat in the water column remains constant during the mixing phase, the transition from convex to a more linear profile is associated with the increase of temperature at the level of the SB. Anywhere from 10 to 50 min elapsed between the tow body's passage and temperature measurements being taken inside the wake. This may be sufficient for the long-term, mixing-induced modification of the water column and may be responsible for the observed local increases in temperature (e.g. Figure 6(a)). We readily acknowledge alternative explanations for the observed variability, such as the advection of water masses from the adjacent region, wind-driven effects or the passage of internal waves. Unambiguous validation of the 'hydrodynamic warming' hypothesis requires continuous observations over much longer periods of time, as well as the detailed knowledge of the ambient circulation patterns. Nevertheless, the systematic trends observed during all three days of field experimentation are suggestive, stimulating, and deserve further investigation. If validated, the variation in mean-field profiles could be potentially exploited for detection purposes.
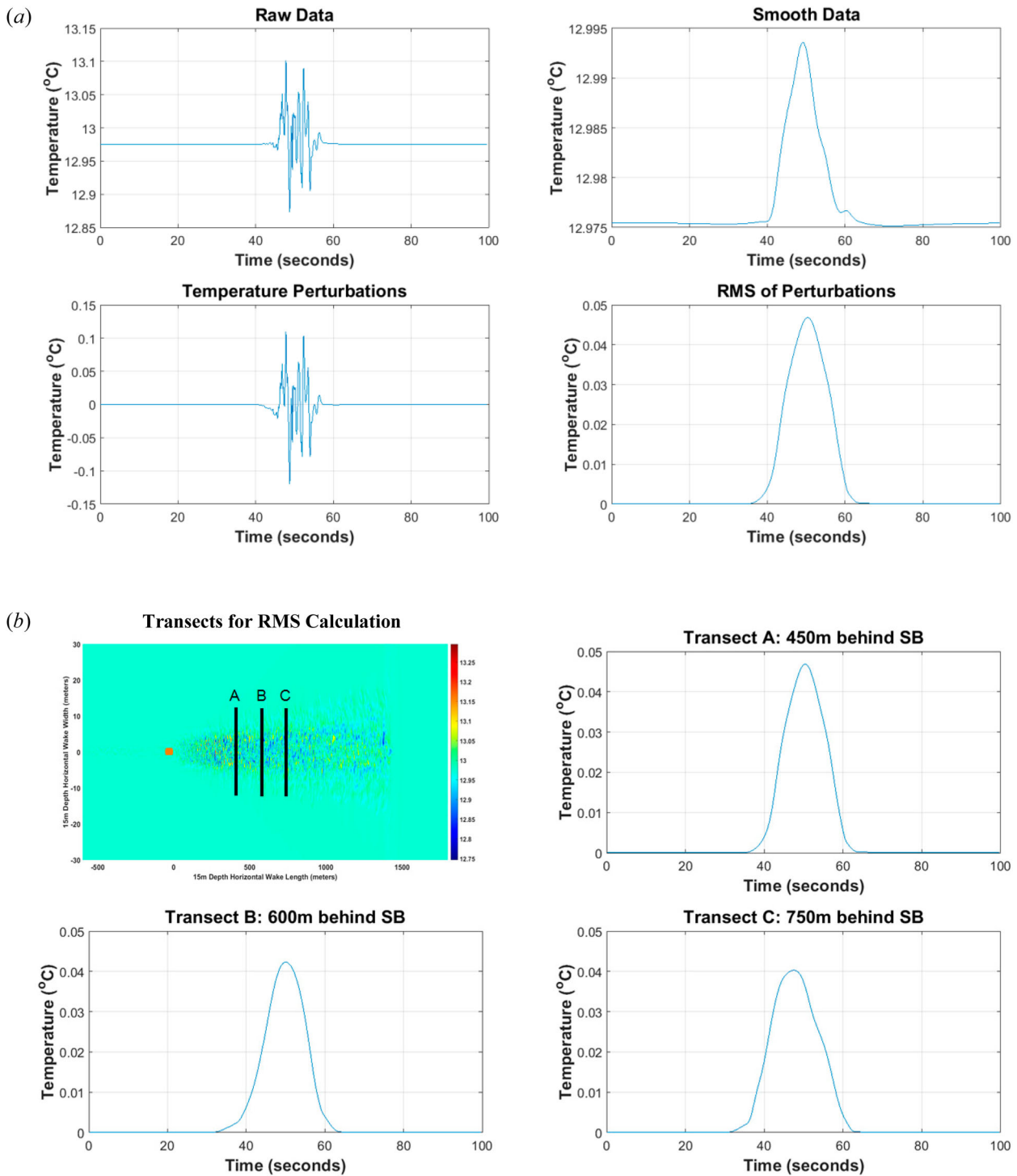
(a)

(b)

Figure 4. (a) Conversion of the temperature data to RMS perturbations. (b) Synthetic REMUS transects: horizontal temperature pattern at 15 m depth level for $t = 480$ s. and T_{rms} calculated along sections A, B, and C, which correspond to 450, 600, and 750 m behind the SB accordingly.

3.2. Horizontal variability of temperature

The third and final field test was conducted on 28 August 2015 utilising the *RV John Martin* and the Naval Post-graduate School's Rigid Hull Inflatable Boat (RHIB). The primary goal of the August experiment was to collect

horizontal *in situ* temperature data using a Hydroid REMUS 100 AUV (Figure 5(f)) programmed to make multiple orthogonal passes through the tow body wake. The REMUS is equipped with a YSI 600 XL temperature sensor which has a range of −5 to 50°C and resolution of 0.01°C. The *RV John Martin* was used as the tow vessel
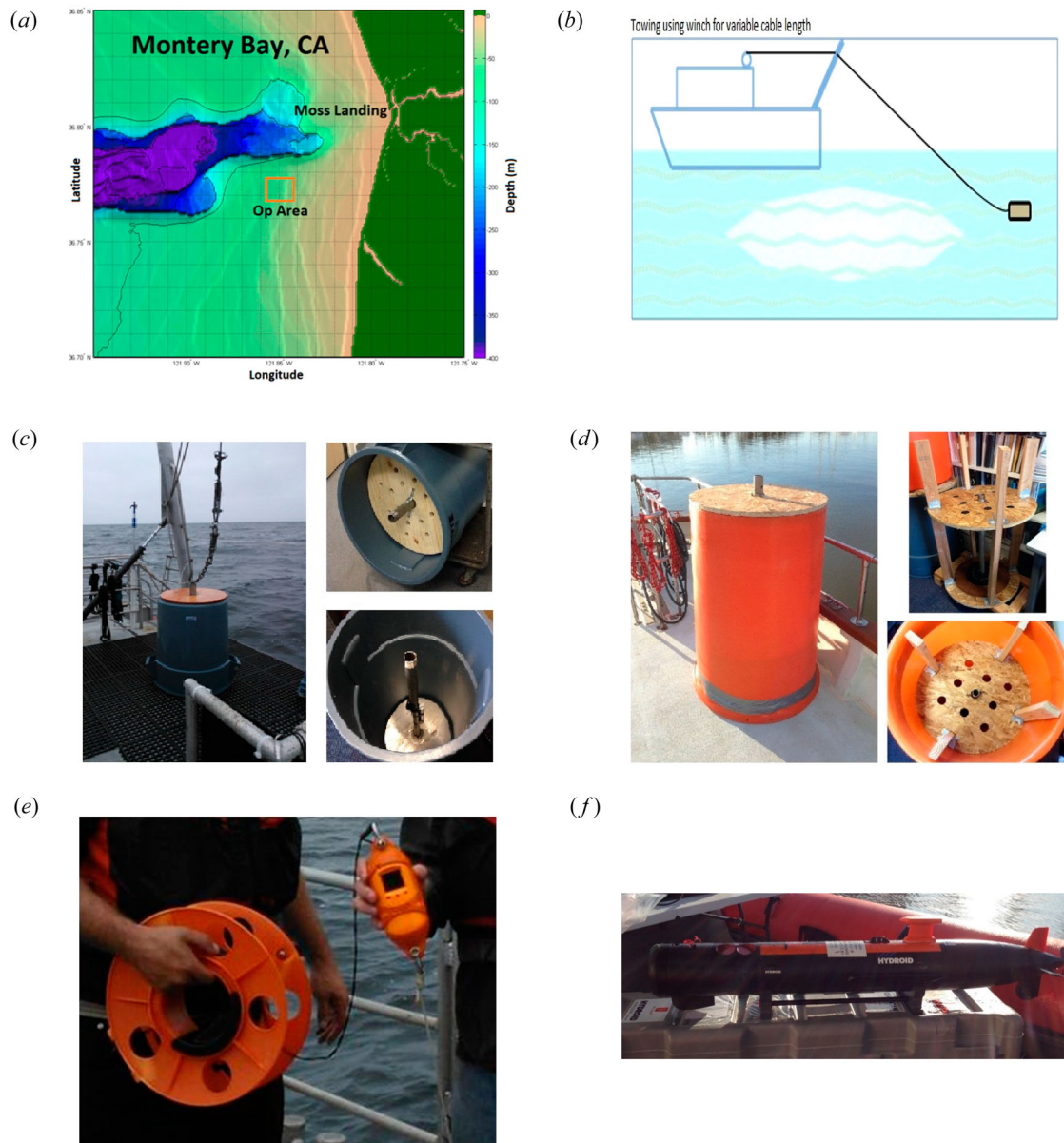
Figure 5. Field project. (a) Operating area within Monterey Bay, CA (orange box). (b) Schematic of the experimental setup. (c) Brute Grey tow body. (d) Agent Orange tow body. (e) SonTek CastAway®-CTD. (f) Hydroid REMUS 100.

and the RHIB was used to launch and recover the REMUS. First, the *Martin* conducted a northeasterly Control run at 6 kt without a SB deployed to examine any effects the tow vessel wake might have on the natural temperature variations within the water column. Upon completion of the *Martin* track, REMUS was launched from the NPS RHIB. REMUS was programmed to initially conduct a compass navigation calibration circle upon release, dive to 15 m, collect *in situ* temperature along the pre-determined track while moving at ~1.5 m/s, and then surface for recovery. REMUS successfully completed this programmed mission in approximately 45 min making six crossings of the *Martin's* track. Next, another 6 kt northeasterly run was

made by the *Martin*, but this time towing Agent Orange at the intended depth of 15 m. Once the 175 m long tow was clear of the operating area, REMUS was launched from the RHIB and again successfully executed the same pre-programmed mission (Figure 7).

During the tow experiment for REMUS measurements, the ship speed was 6 kt with 175 m of cable extended for a target tow depth of 15 m, but it was found that Agent Orange averaged a depth of 13.6 m. For both the Control run and Agent Orange run on 28 August 2015, REMUS recorded *in situ* temperature at 15 m depth along its path. Particular interest was placed on the locations in time where REMUS crossed over the *Martin* tow tracks. In Figure 8, temperature
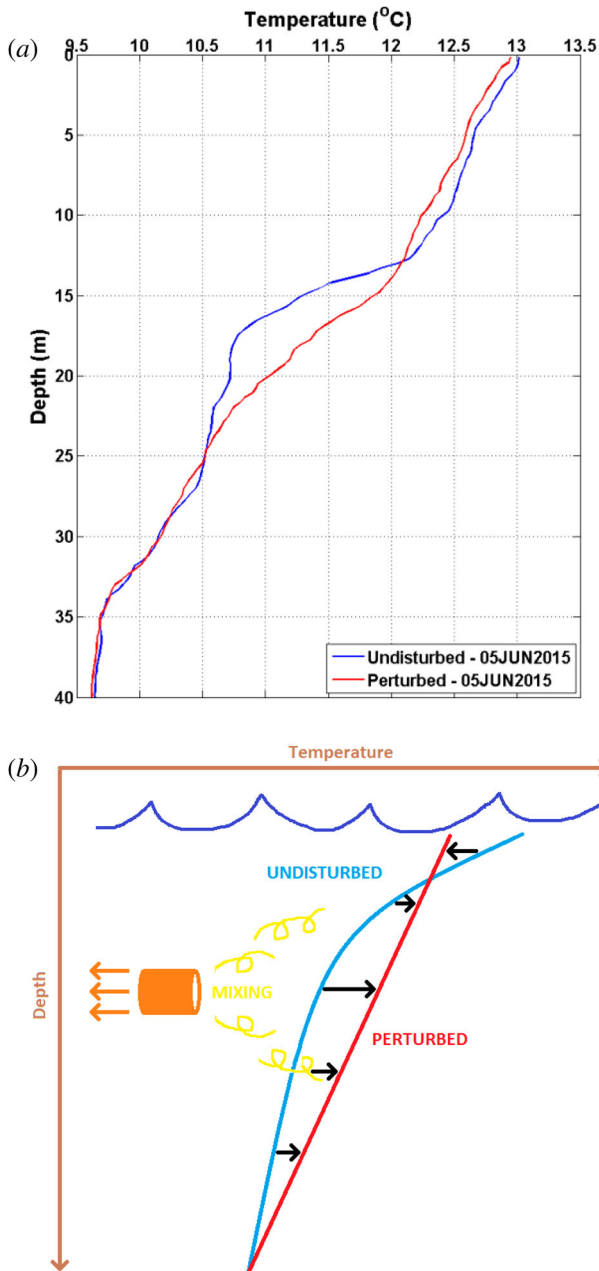
Figure 6. (a) CTD profiles from 5 June 2015. Blue indicates undisturbed water column. Red indicates water column in same region following a 5 kt tow with Brute Grey at 17.0 m depth. (b) Dynamical interpretation of the hydrodynamically induced warming at the level of SB.

perturbations are shown along the track with highlighted regions indicating ~20 m regions of REMUS/*Martin* track crossover locations. Root mean square temperature deviations (T_{rms}) were calculated using REMUS raw temperature data for both the Control and Agent Orange runs in a similar fashion as was done for the DNS results (Section 2). Figure 8(a) presents the Control run, and the actual tow-body experiment (the Agent Orange run) is shown in Figure 8(b). These temperature perturbations

were analysed for magnitude and correlation to track crossover locations. As in the case of numerical simulations, our key diagnostic variable is the RMS. temperature perturbation (T_{rms}) which was computed using the algorithm detailed in Section 2. Importantly, for the Agent Orange run, six sharp increases of in T_{rms} were observed roughly corresponding to where the REMUS crossed through the SB wake regions. The average strength of the signal within the crossing regions (highlighted in Figure 8(b)) exceeded the average signal outside of the wake by $\Delta T_{rms} = 0.05°C$, which is comparable to the variation realised in the numerical experiment (Section 2).

The two-tailed student t-test was used to analyse the statistical significance of RMS temperature within a 20 m region of each wake crossing for both the Control and Agent Orange runs. This test was applied because the crossing region T_{rms} and mean T_{rms} populations are of different sizes with different variances (Welch's t-test). The 20 m 'window' is a conservative length scale to capture the entire width of the wake as the numerically derived turbulent wake stretched ~10 m in the horizontal. Using a larger window allows for sensing areas of increased T_{rms} that may not remain directly in the location in which it was first generated, due to advection from currents. Temperature data at the beginning and end of each time-series were omitted to avoid the contamination of data by the increase in T_{rms} associated with the initial dive and final surfacing.

A statistical test was conducted based on a null hypothesis that mean T_{rms} in the wake region is the same as outside. For the Agent Orange run, with a 95% confidence interval and type one error rate of 5%, the null hypothesis can be rejected with 81.5% probability. Therefore, the T_{rms} sample populations inside and outside the wake region are different in the Agent Orange run. For the Control run, the mean T_{rms} sample populations inside and outside the wake regions were not statistically different. This implies that the tow vessel itself (*RV John Martin*) did not impact temperature measurements at 15 m depth. It should be noted that the main experiment was performed 2.5 h after the Control run (which did not produce systematic internal signals) thus precluding any possibility of cross-contamination of the experimental results.

4. Laboratory experiments

The third component of the presented study is based on a series of laboratory experiments. These experiments complement our field observations (Section 3) by making it possible to perform measurements that would be logistically prohibitive in the ocean. In particular, we
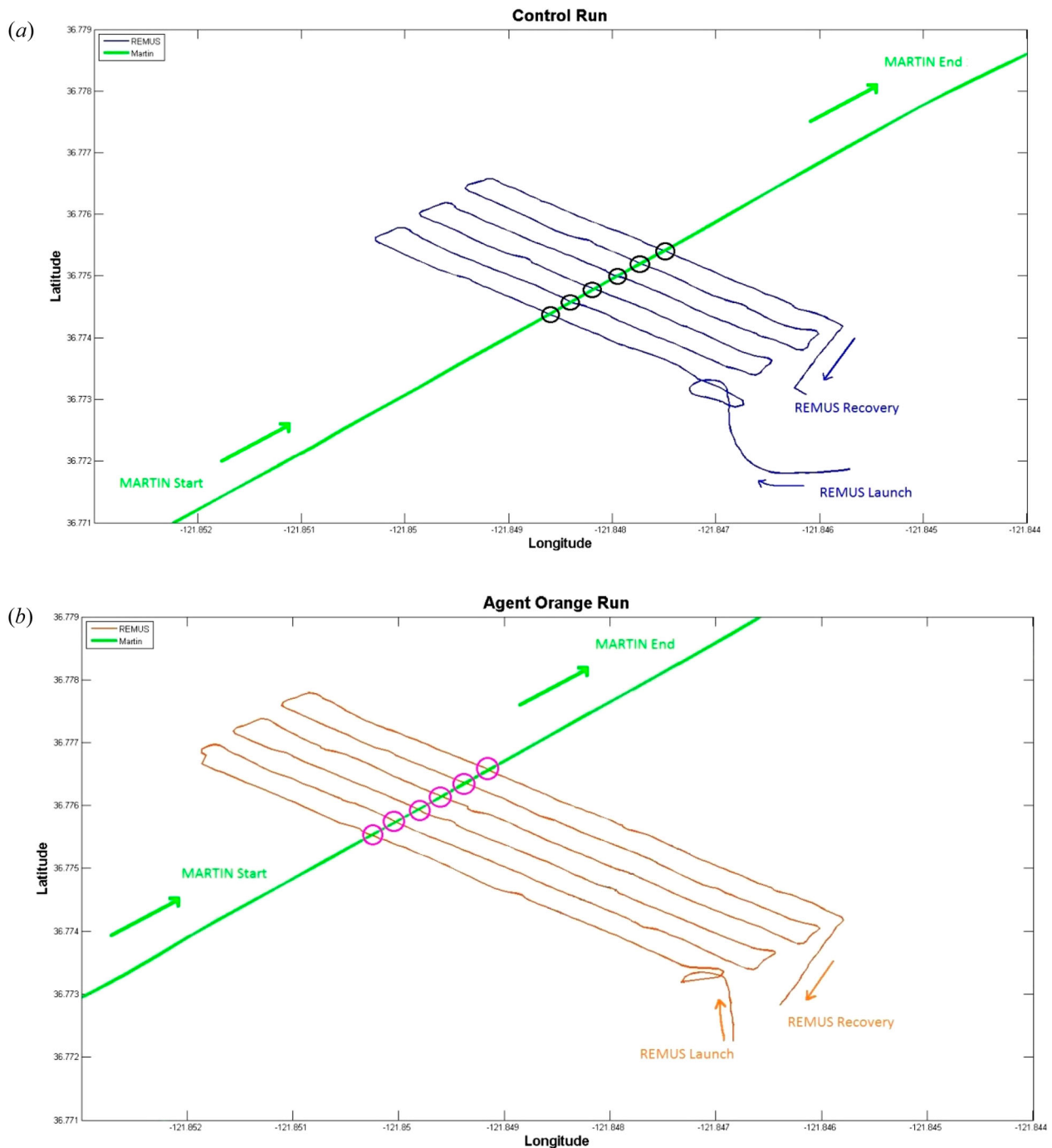
Figure 7. REMUS operations. (a) Control run with Martin and REMUS tracks, black circles indicating crossover locations. (b) Agent Orange run with Martin and REMUS tracks, magenta circles indicating crossover locations.

shall focus our analysis on the conditions of wake surfacing. In the context of our field programme, the accurate two-dimensional mapping of the thermal surface signatures of a wake would require aerial-based measurements. In contrast, surface signatures can be easily and reliably identified in the lab using an IR camera mounted above the tank. It should also be emphasised that physical dimensions of the SB and the associated wake in the lab are incommensurate with scales realised in

operational scenarios. However the key dynamic properties of wakes, which are set by governing non-dimensional numbers (Fr, Re), are likely to be similar in the laboratory and oceanic analogues. Based on our numerical experiments, we assume that, for the specific purpose of determining the *magnitude* of temperature perturbation in the *intermediate* wake, frictional effects are secondary, provided that Re is large. In terms of representative Froude numbers, our laboratory
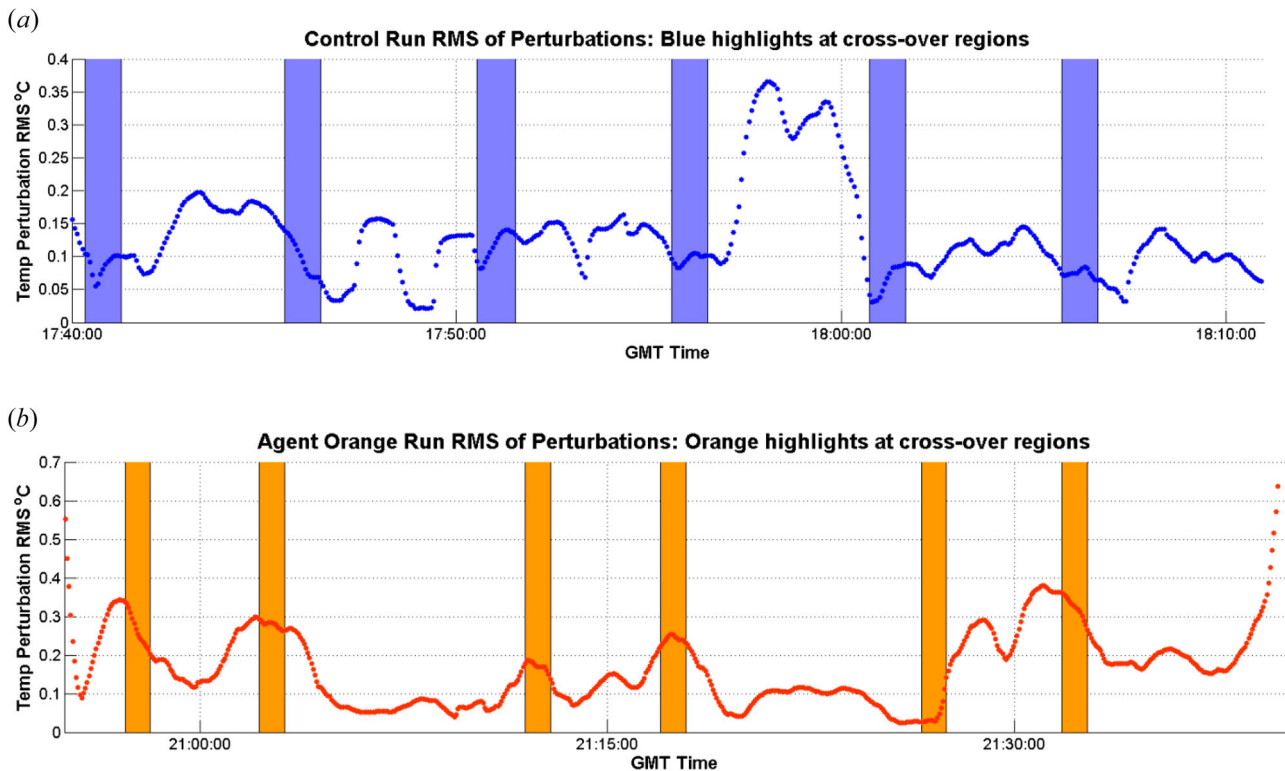
(a)

(b)

Figure 8. REMUS data. (a) RMS temperature perturbations calculated from Control run. Control run crossover regions highlighted in blue. (b) RMS temperature perturbations calculated from Agent Orange run. Agent Orange run crossover regions highlighted in orange.

experiments are designed to match both typical operational conditions and the Monterey Bay experiment (Table 1).

The experiments were performed using a laboratory tank (Merriam 2015) with a poly vinyl chloride (PVC) shuttle to simulate a towed SB as shown in the schematic diagram in Figure 9(a). A two-layer stratified system was set up as follows. First, the tank was filled with ambient room temperature fresh water to depths of 10, 12, or 15 cm, which formed the upper layer. The lower layer was created by adding cooler water with temperature approximately 6°C below ambient to the bottom of the tank. As a result, the warmer layer floated for a total water depth of 30 cm. Shuttle depth was set to coincide with the high-gradient thermal interface between the two layers and a series of runs were conducted by systematically varying the shuttle velocity. An IR camera was focused on the surface of the top water layer to record wake signatures generated by the moving shuttle and a thermistor temperature probe was used within the tank to record temperature at different depths.

The acrylic-walled tank was accessible through the top opening, which allowed for modification of equipment and instrument observations. A thin aluminium rod was suspended horizontally above the tank bottom to provide a guide for the shuttle. Fishing line within a weighted pulley system was implemented to pull the

shuttle along the boundary at the depth between the stratified water layers. Velocity was measured using the movement of a foam block through two photogates (Figure 9(a)). Internal waves generated by the motion of the shuttle were dampened by 8 cm thick, medium density Matala filters at either end of the tank. The wake was visualised by adding green dye to the lower layer. The observed wake signatures exhibited the three evolution phases: turbulent mixing, horizontal expansion, and decay – the pattern which is consistent with most laboratory studies of stratified wakes (e.g. Afanasyev & Korabel 2006). While the shuttle traversed the tank in the span of a few seconds, some runs produced horizontal vortices lasting over 2 min.

For each upper layer depth, the shuttle velocity was gradually increased, which allowed us to evaluate the critical velocity associated with the appearance of surface temperature perturbations detectable by the IR camera. Of the 44 shuttle runs completed, 7 out of 17 (41%) at 10 cm depth, 6 out of 18 (33%) at 12 cm depth, and only 1 out of 9 (11%) at 15 cm depth produced detectable surface signatures. An example of a detectable signal from a 0.476 m/s shuttle run performed at a 10 cm depth is shown in Figure 9(b). The Froude numbers corresponding to the critical velocity (U_{cr}) were plotted against their respective depth ratio, revealing a strikingly linear relationship (Figure 10), which can be described
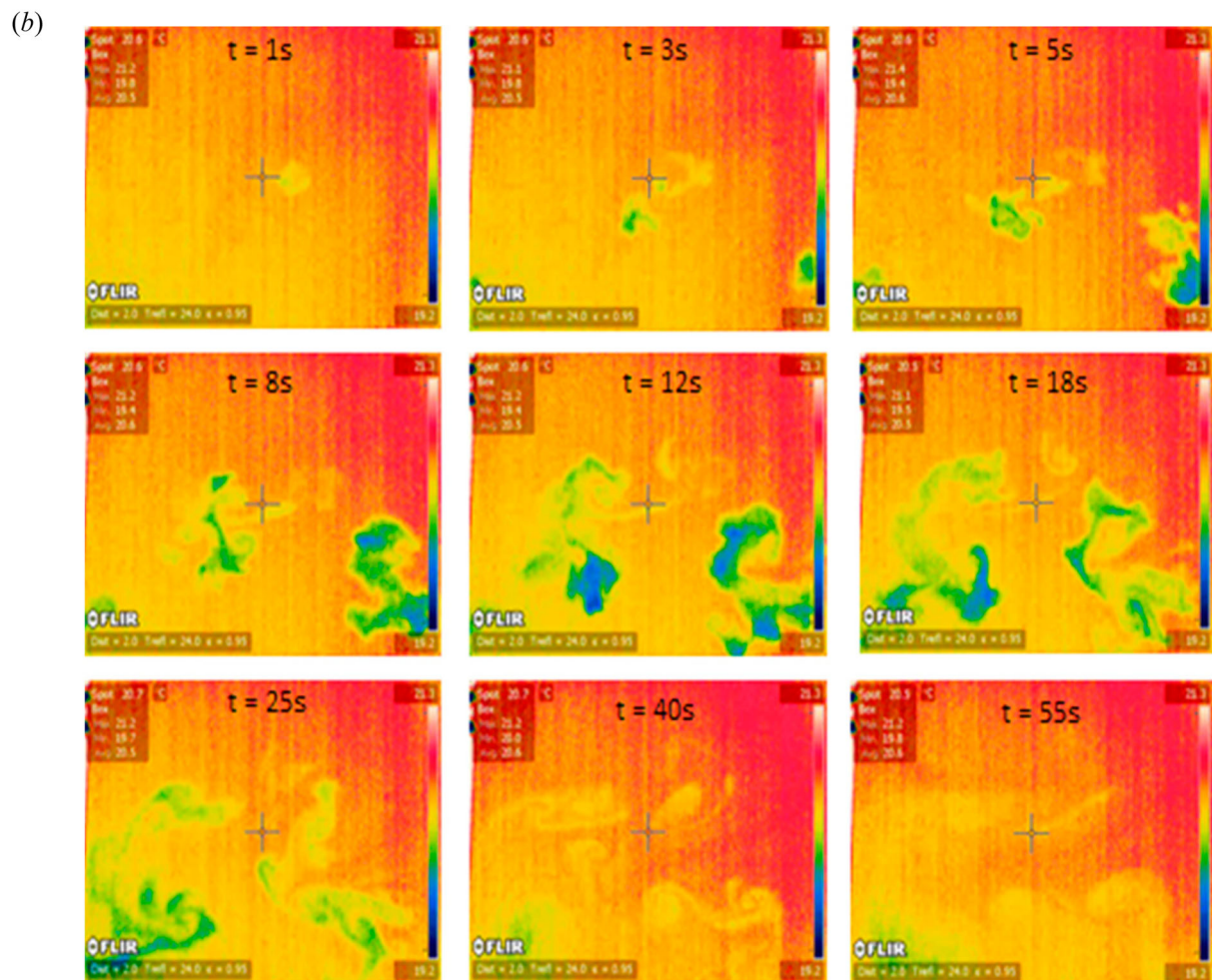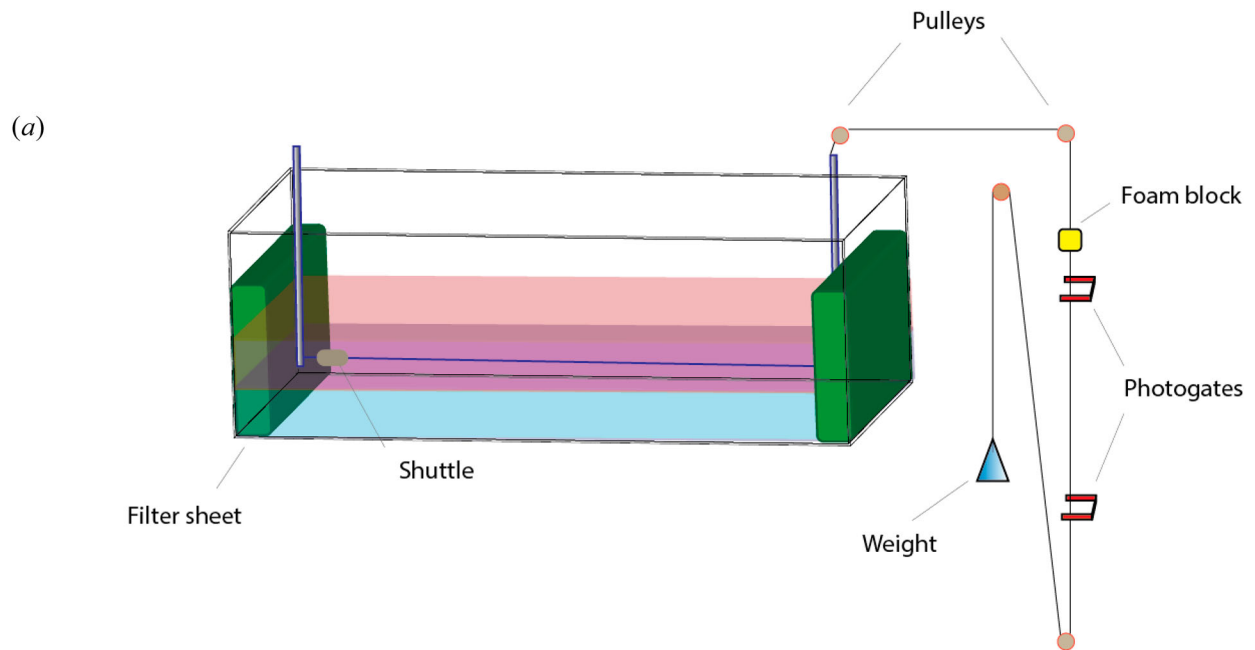
Figure 9. (a) Tank experiment layout. An acrylic-walled tank (183 cm × 61 cm × 61 cm) was filled with two layers of water of different temperature. The SB was towed across the tank by weights attached to the fishing line routed through a series of pulleys. (b) Sequence of IR images for the run at SB depth of 10 cm with the velocity of 0.476 m/s. The series begins 1 s after initial signal detection and progresses through to signal loss.

by the empirical expression:

$$\frac{U_{cr}}{ND} = 268.87\frac{H}{D} - 569.18. \qquad (7)$$

The extrapolation of the prediction Equation (7) to typical operational conditions (Table 1) is suggestive. For instance, a submersible propagating at the speed of $U = 10$ m/s or faster, can be reliably detected from the surface temperature patterns for $H < 35$ m. While such estimates are comparable to the predictions based on numerical simulations (e.g. Martin 2016), they tend to underestimate the detectability depth approximately by a factor of two. This tendency is tentatively attributed to the damping effects of molecular diffusion and viscosity in lab experiments, associated with relatively lower Reynolds and Peclet numbers – effects that are largely negligible in operational conditions.

5. Discussion

This study presents an analysis of the intermediate wakes generated from a towed SB using a combination of numerical modelling, field measurements, and laboratory experiments. The geographic location of the field work is characterised by high stratification and a shallow thermocline, which offers an attractive opportunity to investigate a scaled-down counterpart of realistic scenarios. Laboratory analysis further extended this investigation by presenting the observations that could be logistically prohibitive in field experiments. Numerical modelling helped to interpret results from all methods of experimentation.
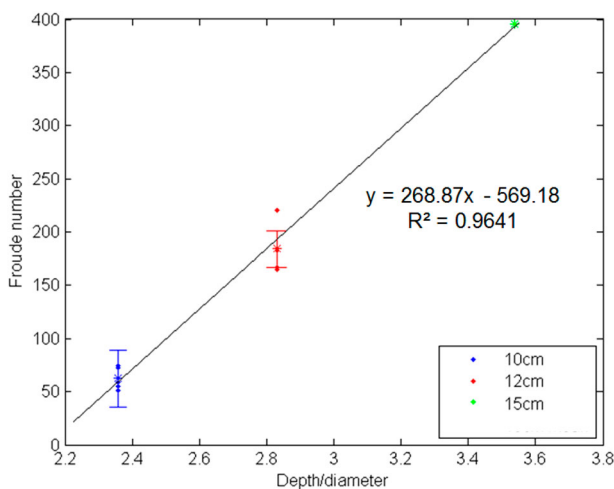

Figure 10. Plot of critical Froude numbers vs. depth ratios. Blue values are from SBs at 10 cm, red indicates 12 cm SB depth, and green indicates 15 cm SB depth, shown with standard error.

Numerical experiments (Section 2) show a distinct 10 m radial wake signature developing at 10–20 m depth range over the course of 125–250 s. The temperature perturbation patterns are characterised by a high degree of variability with warm and cold eddies left behind the SB. This variability was quantified by analysing the perturbation temperature variance in the horizontal transects normal to the wake, which was referred to as the synthetic REMUS data-series. Raw synthetic REMUS data from a modelled wake crossover shows temperature variations between ~12.9°C and 13.1°C. The corresponding T_{rms} deviations, display a 0.047°C peak magnitude at the time of wake crossing and the T_{rms} signal monotonically decays away from the crossing.

The model results are generally consistent with the field data from the Monterey Bay experiments. The field data reveal temperature variations on the order of ±0.15°C and the corresponding T_{rms} deviations show an average increase of 0.055°C within wake regions. The influence from a tow ship was proven to be statistically negligible. The wake signatures realised in simulations were generally less pronounced than in the ocean. However, the quantitative differences may be readily attributed to the idealised model configuration and the limited resolution of the wake relative to the fine scales of turbulence realised in the ocean. At the same time, these differences reinforce our belief that numerical and laboratory investigations should not be viewed as a substitute for the field experiments. The *in situ* wake observations are relatively rare (e.g. Fiekas 1997) and they should be given priority as the source of information for development of the actual detection algorithms.

Another suggestive observation from the field experiment was the persistent long-term change in the stratification following the passage of the SB – the 'hydrodynamic warming' effect (Section 3.1). This proposition, particularly the assumed link between the wake-induced mixing and the reorganisation of mean temperature structure, is somewhat speculative. More effort is required to delineate wake-induced effects from the ambient influences, such as the advection by ocean currents, wind-driven motions, and internal waves. Nevertheless, these observations could open a new and exciting avenue of exploration. The wake-induced changes in highly non-uniform stratification deserve further investigation and could be potentially exploited for detection purposes.

The laboratory component of this project continued our inquiry into hydrodynamic detectability of submerged propagating objects for given background stratification, SB velocity, depth, and size. The laboratory

experiments (Section 4) were focused on the possibility of detection using the surface thermal signal. The systematic variation of the SB speed allowed us to establish a simple empirical relation for the critical velocity of a SB resulting in the appearance of a well-defined thermal surface signature. Despite considerable differences in scales between the laboratory, field experiments, and operational conditions (Table 1) the results and predictions were generally consistent with each other.

An overreaching conclusion from all lines of research used in this study is that hydrodynamically based detection of a wake produced by a propagating submerged object in a stratified fluid is possible. These non-traditional techniques can be used either independently or in conjunction with other well-known means of propagating submersible detection, such as acoustic target location. The project can and should be further developed in several directions. Additional experiments are necessary in order to explore different SB characteristics and environmental parameters which will ultimately lead to development of a general predictive algorithm. The manoeuvring and acceleration of the SB was not taken into consideration, but would most likely (e.g. Voropayev et al. 1999) result in the amplification of both interior and surface signatures of the wake. Extending the period of observation into the late wake regime, while continuing to monitor the interior thermal signal, will make it possible to quantify the decay rates of turbulent patches – an important problem of general oceanographic significance. The proposed critical conditions for the surfacing of a wake need further refinement and inter-comparison between numerical, observational, and laboratory analogues. Nevertheless, even our preliminary results indicate that detection based on thermal wake signatures is highly promising as a means of non-acoustic target recognition.

Acknowledgements

Disclosure statement

Funding

ORCID

Timour Radko 🔟 http://orcid.org/0000-0002-5682-280X
John Joseph 🔟 http://orcid.org/0000-0001-9267-9118

References

Afanasyev YD, Korabel VN. 2006. Wakes and vortex streets generated by translating force and force doublet: laboratory experiments. J Fluid Mech. 553:119. doi:10.1017/S0022112006008986.

Fiekas H-V. 1997. Experimental investigations inside the turbulent wake of a submerged submarine. Hamburg: UDT 97.

Han TY, Menj JCS, Innis GE. 1983. An open boundary condition for incompressible stratified flows. J Comput Phys. 49:276–297.

Lin JT, Pao YH. 1979. Wakes in stratified fluids. Ann Rev Fluid Mech. 11:317–338.

Marshall J, Adcroft A, Hill C, Perelman L, Heisey C. 1997. A finite-volume, incompressible Navier Stokes model for studies of the ocean on parallel computers. J Geophys Res. 102:5753–5766.

Martin MA. 2016. Influence of momentum excess on the pattern and dynamics of intermediate-range stratified wakes [Master's thesis]. Dept. of Oceanography, Naval Postgraduate School, 121 pp.

Merriam CJ. 2015. Laboratory experiments on stratified wakes [Master's thesis]. Dept. of Oceanography, Naval Postgraduate School, 57 pp.

Meunier P, Spedding GR. 2004. A loss of memory in stratified momentum wakes. Phys Fluids. 16:298–305.

Orlanksi I. 1976. A simple boundary condition for unbounded hyperbolic flows. J Comput Phys. 21:251–269.

Radko T. 2001. Ship waves in a stratified fluid. J Ship Res. 45:1–12.

Redford JA, Lund TS, Coleman GN. 2015. A numerical study of weakly stratified turbulent wake. J Fluid Mech. 776:568–609.

Schooley AH, Stewart RW. 1963. Experiments with a self-propelled body submerged in a fluid with a vertical density gradient. J Fluid Mech. 15:83–96.

Spedding GR. 2014. Wake signature detection. Annu Rev Fluid Mech. 46:273–302.

Spedding GR, Browand FK, Fincham AM. 1996. Turbulence, similarity scaling and vortex geometry in the wake of a towed sphere in a stably stratified fluid. J Fluid Mech. 314:55–103.

de Stadler MB, Sarkar S. 2012. Simulation of a propelled wake with moderate excess momentum in a stratified fluid. J Fluid Mech. 692:28–52.

Voropayev SI, Fernando HJS, Smirnov SA, Morrison R. 2007. On surface signatures generated by submerged momentum sources. Phys Fluids. 19:076603. doi:10.1063/1.2749713.

Voropayev SI, McEachern GB, Fernando HJS, Boyer DL. 1999. Large vortex structures behind a maneuvering body in stratified fluids. Phys Fluids. 11:1682–1684.

Voropayev SI, Nath C, Fernando HJS. 2012. Thermal surface signatures of ship propeller wakes in stratified waters. Phys Fluids. 24:116603. doi:10.1063/1.4767130.

Voropayev SI, Smirnov SA. 2003. Vortex streets generated by a moving momentum source in a stratified fluid. Phys Fluids. 15:618–624.